Medical Engineering and Physics 68 (2019) 101–107

Contents lists available at ScienceDirect

Medical Engineering and Physics

journal homepage: www.elsevier.com/locate/medengphy

Technical note

A portable bioimpedance instrument for monitoring residual limb fluid volume in people with transtibial limb loss: A technical note

Paul Hinrichs, John C. Cagle, Joan E. Sanders*

Department of Bioengineering, University of Washington, 355061, 3720 15th Ave NE, Seattle WA 98195, United States

ARTICLE INFO

Article history:
Received 20 April 2018
Revised 4 March 2019
Accepted 3 April 2019

Keywords:
Bioimpedance
Amputee
Residual limb
Fluid volume
Prosthetic fit
Volume accommodation

ABSTRACT

People with transtibial limb loss experience daily changes in volume of their residual limb that affect the fit of their prosthetic socket. A portable instrument was developed to monitor fluid volume changes outside of the laboratory setting. The bioimpedance system applied 26 current bursts per second at frequencies between 3 kHz and 1 MHz, and sensed voltage at up to six channels. Among six voltage-controlled current source circuits and five receive-channel amplifier topologies considered, a differential Howland current pump and a single receive-channel instrumentation amplifier proved the best combination of low noise and low power consumption. Mean RMS errors were 0.07% for extracellular fluid resistance, 2.23% for intracellular fluid resistance, and 1.15% for membrane capacitance.

1. Introduction

Changes in prosthetic socket fit due to changes in residual limb volume are the most important challenge faced by people with limb loss [1]. When the limb changes size, stresses at the limb-socket interface support the residual limb differently. Focused stresses may be created and put soft tissues at risk of trauma. A loose socket may be unstable and cause the prosthesis user to fall. Daily volume changes occur as a result of an imbalance between fluid entering and leaving the residual limb, particularly extracellular fluid within the interstitial space [2]. Even a socket that is oversized just 1% may induce a clinically detectable change in socket fit [3].

Researchers have monitored residual limb fluid volumes in laboratory investigations to gain insight into how prosthetic componentry and actions by users affect them [4–8]. A custom-designed stationary biompedance analysis system was used for monitoring transtibial amputee participants while they stood, sat, and walked on a treadmill [9]. While this instrument helped provide important insight under controlled laboratory conditions, its lack of portability made it incapable of long-term monitoring in free-living environments, a next step in clinical research investigation.

The purpose of this effort was to extend from the prior instrument to create a portable bioimpedance monitoring unit to measure limb fluid volume changes over the day while a participant with transtibial limb loss walked outside of the laboratory. In this Technical Note, test results using different circuit designs are reported, and the final design of the instrument is described.

2. Instrumentation

The instrument was designed to assess limb fluid volume change in people with transtibial amputation by measuring change in the impedance of the residual limb over time. It was interfaced to the residual limb through thin electrodes developed specifically for this purpose [9]. The electrodes were made using thin (0.09-mm thickness) electrically conductive tape (ARCare 8881, Adhesives Research Incorporated, Glen Rock, Pennsylvania) and an underlying hydrogel (9880, 3 M). Participants reported previously that the electrodes felt comfortable and wore them for hours during testing [4]. A sturdy disposable connector (Fischer Disposable Series, Fischer Connectors, Alpharetta, Georgia) was used to connect lead wires (custom 32AWG, 7-stranded wire,

Abbreviations: α, correction term; μSD, micro SD card; ρ_e, resistivity of extracellular fluid; ADC, analog to digital converter; C, mean circumference of the residual limb; C_m, membrane capacitance; CMR, common mode signal rejection; DAC, digital to analog converter; FPGA, field-programmable gate array; I, resistive component of bioimpedance; L, distance between voltage-sensing electrodes; *Msps*, megasamples per second; Q, reactance component of bioimpedance; R_e, extracellular fluid resistance; R_i, intracellular fluid resistance; RMS, root mean square; T_d, transmission delay term; USB, universal serial bus; V_e, extracellular fluid volume; VCCS, voltage controlled current source; Z_{distal}, impedance between the distal voltage-sensing and distal current-injecting electrodes; Z_n, Impedance in channel n; Z^{obs}, Observed complex impedance; Z_{thigh}, Impedance between the proximal voltage-sensing and proximal current-injecting electrodes.

* Corresponding author.
E-mail address: jsanders@u.washington.edu (J.E. Sanders).

https://doi.org/10.1016/j.medengphy.2019.04.002
1350-4533/

New England Wire Technology, Lisbon, New Hampshire) to the system electronics, and an adhesive was used to affix lead wires to electrodes (+PLUSeries Composite 1-Minute Adhesive, FabTech Systems, Everett, Washington). Impedance was determined by injecting a known sinusoidal current through the limb at selected frequencies, and measuring the resulting voltage across locations on the anterior lateral and posterior residual limb surfaces (Fig. 1a) (four-wire Kelvin sensing arrangement) (Appendix 1). The voltage and current wave forms were demodulated to produce the real and complex components of the measured impedance.

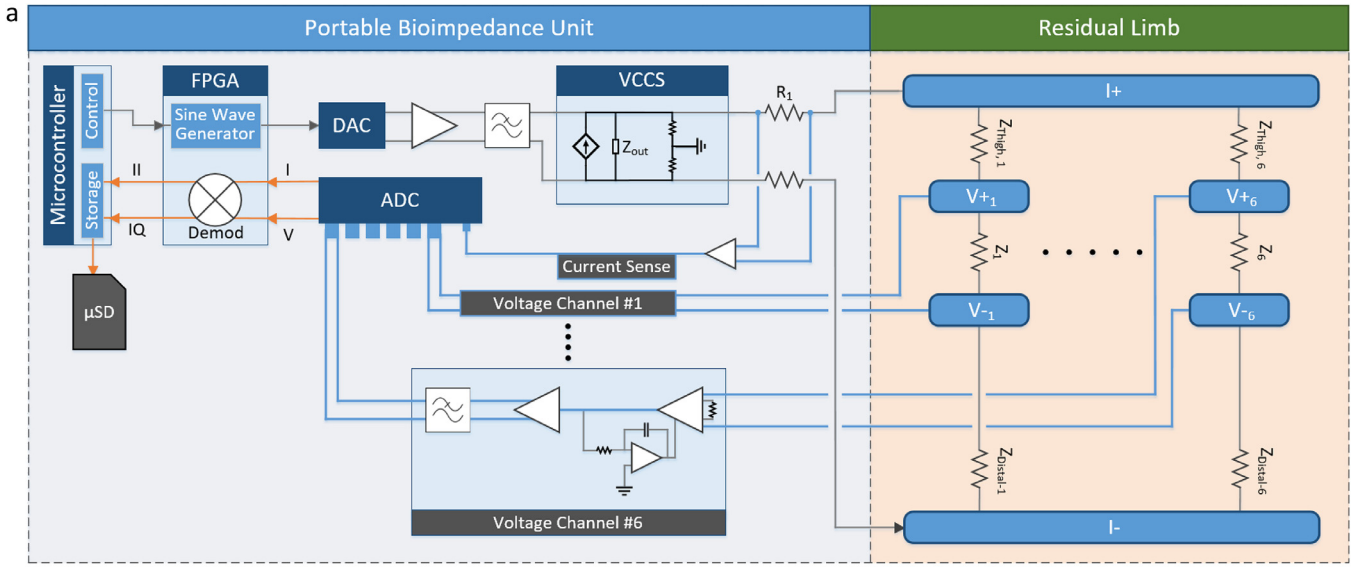

Fig. 1. Measurement system. (a) Electronic components of the portable limb fluid volume monitoring instrument are shown on the left. Up to six channels of impedance (Z_1 .. Z_6) are monitored. Thigh and distal residual limb impedances (Z_{thigh} and Z_{distal}, respectively) are included because they must be accounted for in data processing. Between the DAC and VCCS there are two filters. The first filter is an active third order low-pass filter integrated into a fully differential amplifier with a cutoff frequency of 15 MHz. The differential output of this is fed into the second filter, which is a passive low pass filter (balanced Chebyshev Type II with the filter zero at 24 MHz). (b) System in use on a person with transtibial limb amputation.

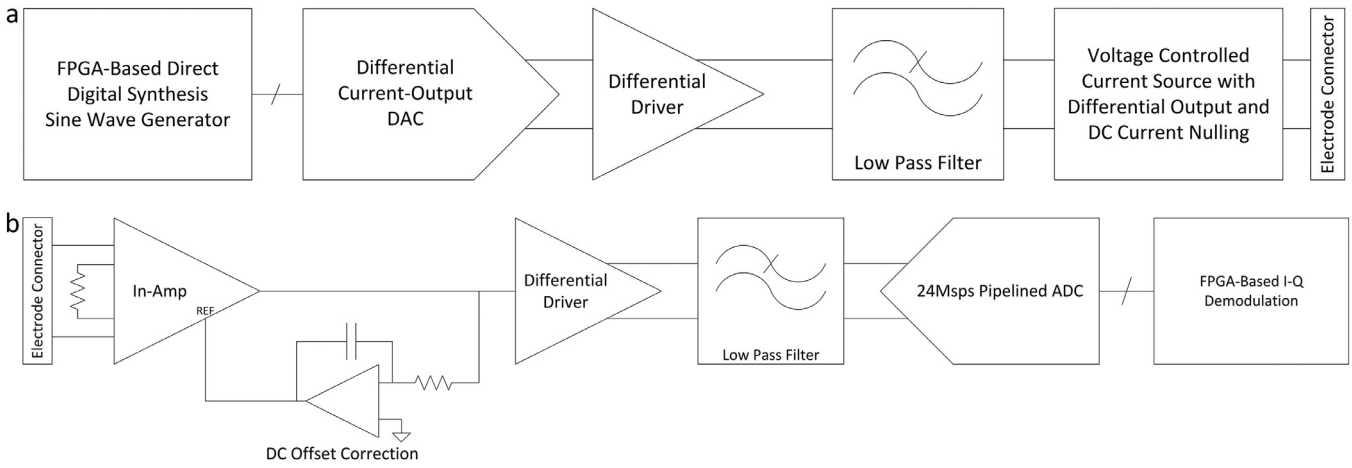

Fig. 2. Current stimulation and voltage sensing circuits. a: Current stimulation components. b: Voltage sensing components.

2.1. Current source

The current source was a novel implementation of the Improved Howland voltage-controlled current source (VCCS) [10], using a fully differential driver and adding DC nulling to eliminate steady state offset currents. The output signal was integrated and fed back to the driver to reduce common-mode offset and DC current to negligible levels. The analog stimulus signal used to drive the VCCS was generated using direct digital synthesis implemented in a field-programmable gate array (FPGA). The digitally synthesized sine wave was converted to an analog signal using conventional digital-to-analog conversion (DAC) techniques before being fed to the VCCS (Fig. 2a).

2.2. Voltage-sense channels

The differential signals for voltage sensing were sensitive and could be afflicted with common-mode offset voltage. Instrumentation amplifiers were selected based on their common-mode rejection and high input impedance (AD8421, Analog Devices). The design was in three parts. Part A consisted of the front-end integrated instrumentation amplifier. Part B was a DC nulling circuit. The DC component at the output of the instrumentation amplifier was integrated and nulled out to remove component mismatch errors and electrode-induced voltage offsets (Fig. 2b). Part C was an integrated differential output driver, which took the ground-referenced (single-ended) output of Part B and turned it into a differential signal.

2.3. Data conversion

Current and voltage sense signals were converted to digital values with the use of a high-speed, pipelined, 8-channel, 12-bit analog-to digital converter (ADC). A 24 MHz sampling frequency was chosen so that the Nyquist frequency of the system was significantly larger than the largest excitation frequency of 1 MHz, in order to maintain reasonable fidelity. For ideal accuracy, the current and voltage signals must be sampled in parallel at the same instant, hence the use of a simultaneous-sampling ADC. Logic in the FPGA compared the measured current and voltage waveforms to determine the impedance relationship.

2.4. Impedance determination

The system applied current as a gated sine wave, sweeping through a set of 26 logarithmically spaced frequencies from 3 kHz to 1 MHz. Each frequency was applied for between 1.0 and 1.7 ms. Including intermission gaps between different frequencies, the entire sweep of frequencies was applied at a rate of 30 Hz in order to properly capture the spectral components of participants' gait [22] (Table 1). The first and last cycles of the applied current waveform were windowed with a ramp function to reduce transients associated with the start and end of the signal. The digitized current and voltage waveforms were multiplied together and averaged over the window to determine the in-phase (resistive or "I") component of the impedance. The digitized current waveform was delayed by ¼ cycle (90°) and multiplied by the digitized voltage waveform to determine the quadrature (reactive or "Q") component of the impedance (Fig. 3).

Table 1
Current injection profile.

Frequency (Hz)	# of Cycle Injected	# of Cycles used in Demodulation
3000	5	3
4000	6	4
5000	7	5
6000	8	6
8000	10	8
10,000	12	10
12,000	15	12
15,000	18	15
20,000	23	20
25,000	25	22
30,000	30	27
40,000	40	36
50,000	50	45
60,000	60	54
80,000	80	72
100,000	100	90
120,000	120	108
150,000	150	135
187,500	188	169
240,000	240	216
300,000	300	270
375,000	375	337
500,000	500	450
600,000	600	540
750,000	755	679
1,000,000	1022	919

2.5. Data logging and communication

A microcontroller was incorporated into the design to manage high-level system tasks. The result of the impedance measurement

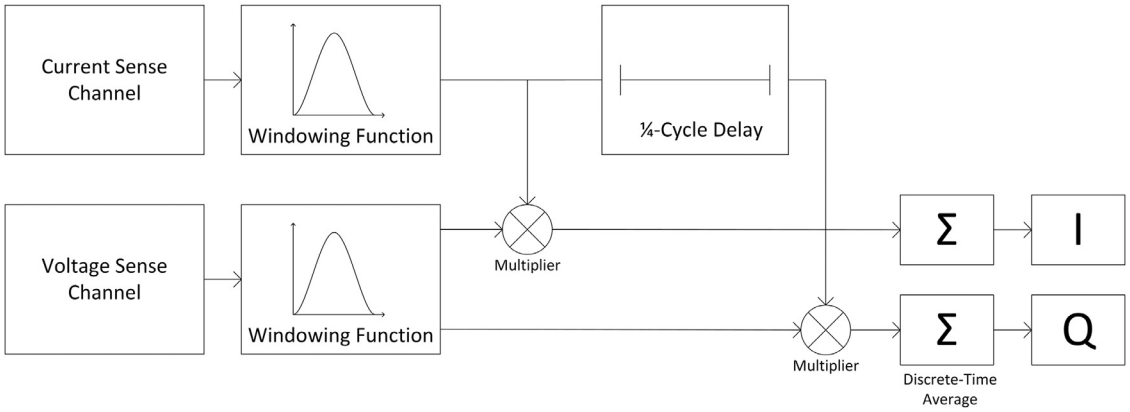

Fig. 3. Determining impedance from collected current and voltage data. I = resistive component. Q = reactive component.

Table 2
Key parts of the portable system.

Part	Description	Manufacturer
LPC4337	ARM Cortex-M4/M0 Microcontroller	NXP, Eindhoven, Netherlands
XC6SLX16	Field-Programmable Gate Array	Xilinx, San Jose, California
CC3100MOD	Wi-Fi Network Processor with Integrated Radio	Texas Instruments, Dallas, Texas
LTC1668	Differential Current-Output Digital-to-Analog Converter	Linear Technology, Milpitas California
AD9637-40	40Msps, 8-Channel, 12-Bit Analog to Digital Converter	Analog Devices, Norwood, Massachusetts
AD8421A	Low-Power, Wide-Bandwidth, Instrumentation Amplifier	Analog Devices, Norwood, Massachusetts

for each frequency was sent from the FPGA to the microcontroller, which saved it to a μSD memory card for later analysis. The data was also optionally transmitted over a Wi-Fi connection so that data collection sessions could be monitored in real time. The system was set up and controlled through a USB serial interface on the microcontroller.

2.6. Packaging

The circuit assemblies (Table 2) were contained within a housing to shield the electronics from any incidental mechanical contact that might occur while the device was worn. Passive cooling was sufficient since the unit generated little waste heat. Commercially available lithium-ion batteries (6400 mA-h) powered the instrument for approximately 9 h. Longer-term testing was accomplished by periodically swapping out the battery. The final assembly fit on a belt and was of dimension 15 cm × 11 cm × 4 cm and weight 5.3 N, including the battery (Fig. 1b).

2.7. Calibration

Although care was taken in the circuit design to minimize potential sources of error, it was impossible to remove them completely from the system. Periodic calibration was required to verify device functionality and correct systematic errors. Three known impedances (Calibration Circuits in Table 3) were measured that spanned the expected range of limb impedance [9]. Using the actual and measured impedance values, a mathematical transformation described by Bao et al. [11] was implemented to produce three correction coefficients to calibrate data from the instrument, as described in detail in Appendix 2. Quality of the calibration was tested using a second set of three known impedances (Check Circuits in Table 3). During calibration and testing, other impedances were placed between the current source electrodes and the sensing electrodes to approximate the impedances of the thigh and distal sections of the residual limb (Fig. 1a). Analysis demonstrated insignificant sensitivity to changes in thigh and distal end resistor and capacitor values over ranges measured on trans-tibial amputee participants, thus only one set of values for thigh and distal end impedance were used during calibration (Appendix 2). To test accuracy, we compared these data and the known impedance values and calculated a root mean square (RMS) error. An external, custom calibration rig that housed these calibration and reference circuits was commanded by the instrument's microcontroller to automate this process (Appendix 2). Gold conductive base plates were used in the calibration rig to hold the electrodes so as to avoid inducing an electric potential between the conductive base plates and the electrically conductive tape of the electrodes. DC rejection in the voltage sense channels minimized remaining electrical potential. A calibration check was run each time the unit was turned on.

Table 3
Calibration and check circuits–nominal values.

Circuit	R_{ecf}	R_{icf}	C_m
Calibration Circuit 1	10 Ω	30.1 Ω	22 nF
Calibration Circuit 2	40.2 Ω	100 Ω	10 nF
Calibration Circuit 3	82.5 Ω	392 Ω	1 nF
Check Circuit 1	36.5 Ω	82.5 Ω	15 nF
Check Circuit 2	48.7 Ω	158 Ω	10 nF
Check Circuit 3	68.1 Ω	280 Ω	3.3 nF

2.8. Cole model

De Lorenzo's form of the Cole model was used to convert impedance data to model physiological components–extracellular and intracellular fluid resistances and membrane capacitance [12]. The model included a time delay term to account for transmission

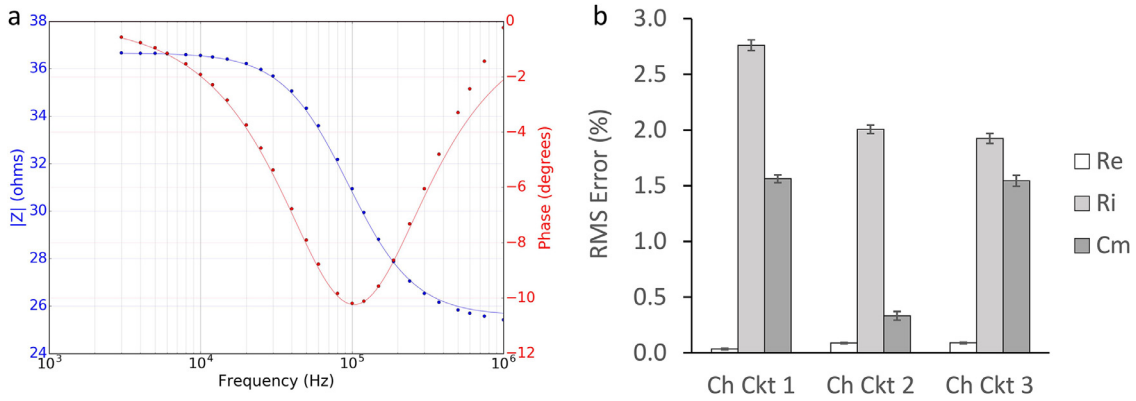

Fig. 4. Performance. a: Cole–DeLorenzo bioimpedance model fitted to impedance data (phase and magnitude). Dots represent the per frequency impedance that is output from calibration. Lines represent the Cole–Delorenzo model fit. b: RMS errors from check circuit testing. Means and standard deviations from 60 sets of data (five circuit boards, four channels on each board, 3 test circuits) are shown. Mean RMS errors were 0.07% for R_e, 2.23% for R_i, and 1.15% for C_m.

Table 4
Results from common-mode rejection tests of circuit topologies tested for use as receive channel amplifiers. Circuits 2 to 5 different from Circuit 1 only in their Part A (integrated instrumentation amplifier) design.

	Topology	Residual CM signal (mV_{RMS} AC)	Residual CM signal (mV_{RMS} DC)	Residual CM signal (mV_{PP})	Approximate Common-mode signal rejection (dB)
1	Single instrumentation amplifier (original circuit)	28.2	28.3	79.4	22
2	Cascaded instrumentation amplifier–dual instrumentation amplifier added and fed into Part A of circuit 1	2.6	2.8	7.3	43
3	Discrete instrumentation amplifier–individual components used (3 op-amps with resistors and capacitors) for Part A	10.0	10.1	28.5	31
4	Discrete instrumentation amplifier with integrated difference amplifier–2 op-amps fed into an integrated difference amplifier for Part A	23.7	23.8	67.8	24
5	Reference high-power high-frequency instrumentation amplifier–used an amplifier with a CMRR specified up to 1 MHz	0.3	1.0	small	52–61

delays through the wires to the electrodes (T_d), and an additional correction term (α). The observed complex impedance was:

$$Z^{obs} = \left(\frac{R_e}{R_e + R_i}\right)\left(R_i + \frac{R_e}{1 + [jwC_m(R_e + R_i)]^{\alpha}}\right)e^{-jwT_d} \quad (1)$$

where R_e is the extracellular fluid resistance, R_i is the intracellular fluid resistance, C_m is the membrane capacitance, and w is frequency.

Fenech and Jaffrin's limb segment model [13], which was an extension from Hanai [14], was then used to convert impedance data to limb fluid volume:

$$V_e = \left(\frac{1}{1000}\right)\left(\frac{\rho_e \times C}{R_e}\right)^{2/3}\left(\frac{L^{5/3}}{(4\pi)^{1/3}}\right) \quad (2)$$

where V_e is the extracellular fluid volume in mL, ρ_e is the resistivity of extracellular fluid in Ω cm, C is the mean circumference of the limb in cm as measured at the V+ and V- electrodes, and L is the distance between the V+ and V- electrodes in cm.

3. Testing and optimization

Results from testing performance of 5 circuit boards (Circuit 1), 4 channels tested on each board, 3 circuits in each test for a total of 60 sets of data, showed very low errors for the primary variable of interest, extracellular fluid resistance R_e. RMS errors for R_e averaged 0.07% (SD 0.03%), for R_i averaged 2.23% (SD 0.38%), and for C_m averaged 1.15% (SD 0.58%). The average R_e error corresponded to a V_e error of 0.04%, assuming a residual limb impedance of 50Ω. Drift in impedance, tested over 24 h, was <0.2% at frequencies below 1 MHz, and <0.08% at frequencies below 200 kHz.

Error in the model fit R_i and C_m values corresponded to degraded measurement accuracy in the signal receive channels at high frequencies (Fig. 4a). With a view on improving performance, four new voltage sensing circuits and five new VCCS circuits were investigated. The new voltage sensing circuits differing from the original circuit (Circuit 1) only in their integrated instrumentation amplifier design. The designs are described in Table 4. New circuit boards were fabricated for each design and the evaluations repeated. A common-mode signal of a 1.06 V_{PP} sine wave at 1 MHz was applied to both inputs of each amplifier. The output signal was measured for each circuit using three different built-in measurement strategies on a digital sampling oscilloscope (MSO-X 4034A, Keysight; N2818A differential probe, Keysight).

Five new VCCS circuits, specifically designed for high frequency performance and thus avoiding the need for matched capacitances, were also tested. The designs, listed in Table 5, were extensions of those described in the literature [15–21]. Each circuit was set up to generate a 1 mA_{RMS} current into a test load consisting of a 49.9 Ω resistor plus a varying load of between 0 and 800 Ω. The output signal voltage across the 49.9 Ω resistor was measured using the digital sampling oscilloscope and differential probe. Output impedance was calculated using a linear least-squares fit to the measured data.

Results from tests of the voltage-sensing circuits demonstrated that, though the new circuits (circuits 2 to 5) improved CMR, there was no corresponding improvement in R_i and C_m accuracy (Table 4). All three measurement methods were in agreement for Circuits 1–4; circuit 5′s residual common-mode signal approached the noise floor for this technique, and measurements were correspondingly less accurate. Thus the drop off in performance at high

Table 5
Results from output impedance tests of voltage-controlled current source (VCCS) circuits.

VCCS circuit	Z_{out} at 10 kHz (kΩ)	Z_{out} at 100 kHz (kΩ)	Z_{out} at 1000 kHz (kΩ)
Differential Howland current pump (original circuit)	484	341	22.5
Bipolar current conveyor	406	440	64.3
Voltage feedback instrumentation amplifier	288	220	19.9
Cascoded transconductance amplifier	*circuit*	*not*	*stable*
Op-amp current conveyor	*circuit*	*not*	*stable*
Voltage feedback instrumentation amplifier with feedback bias current buffer	299	203	10.9

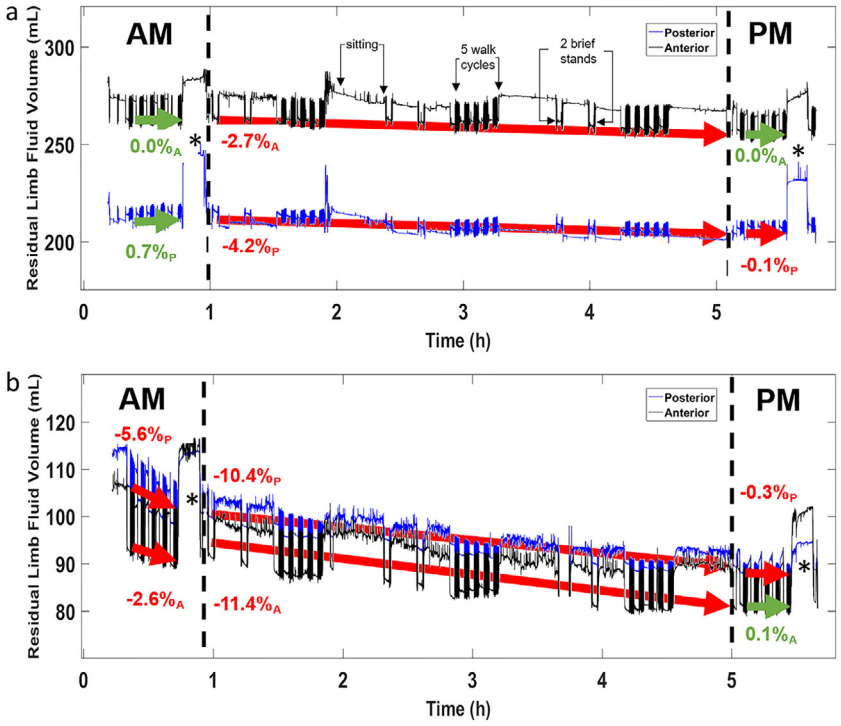

Fig. 5. Participant test data. Results from a test session of >5 h duration conducted in and around a clinical office. a: Participant #1. b: Participant #2. Percent fluid volume changes for the AM, PM, and between-AM-and-PM sections of the test session are shown. An asterisk (*) indicates a doff. A = anterior. P = posterior.

frequencies was not due to characteristics of the receive channel amplifiers but instead from sources elsewhere in the circuit, possibly the VCCS.

For the new VCCS circuits, results showed that circuits using a cascaded transconductance amplifier or an op-amp current conveyor were not stable with representative test loads and were therefore not considered usable (Table 5). Of the four new circuits tested, only the bipolar current conveyor was competitive with the original circuit in performance. Two items were noteworthy. First, the output impedances observed at the maximum frequency of 1 MHz of about 20k Ω were approximately consistent with a high-frequency measurement error of about 5.0%, similar to the errors observed using the original circuit (Fig. 4b). This was an indication that VCCS performance was likely the main limiting factor in overall instrument performance. Second, between the differential Howland current pump (original circuit) and the bipolar current conveyor, neither circuit dominated in performance. The differential Howland current pump was preferable at low frequencies and the bipolar current conveyor performance was superior at high frequencies. However, the advantages of the bipolar current conveyor were modest; it had approximately triple the high-frequency output impedance of the differential Howland current pump, corresponding to roughly a 1.5% measurement error. Considering the increased power consumption and significantly greater complexity of the bipolar current conveyor along with the proven history of the differential Howland current pump, it was judged not worthwhile to replace the differential Howland current pump with the bipolar current conveyor. Because of errors observed at the lowest frequency (3 kHz) and highest frequencies (500 kHz, 750 kHz, 1 MHz), the Cole model was applied over the 5 kHz to 200 MHz frequency range.

4. Example amputee participant data

A test session of duration >5 h was conducted on two people with transtibial limb loss. All procedures were approved by an institutional review board, and written informed consent was obtained before study procedures were initiated (Fig. 5).

Participant #1 was a 53-year old male with a transtibial amputation due to trauma. A high-activity athletic ambulator, this participant spent considerable time standing and ambulating at work. Results show that, as expected from his good health and active lifestyle, this person's residual limb fluid volume was relatively stable throughout the test session. He gained fluid volume during walking segments of the session, consistent with prior results on active participants without peripheral arterial disease tested in the lab [23].

Participant #2 was an 84-year old male who underwent a transtibial amputation 5 years prior due to complication from diabetes (type II). The participant's self-reported health history included high blood pressure and peripheral vascular disease (blood clots) for which he had an inferior vena cava filter. Results show that, as expected because of his peripheral arterial disease, this person underwent limb fluid volume loss over the test session.

4.1. System power measurements

The system consumed 2.5 W during normal operation. This power measurement was about average over the voltage range for a standard lithium polymer battery. The measured 2.5 W power consumption was a significant improvement over the original stationary unit (140 W) [9]. There was not a significant difference between quiescent and active power consumption, since it did not take much energy to drive the Howland circuit. The power consumed was primarily in components in the rest of the system.

5. Conclusion

The developed portable limb fluid volume monitoring instrument is small, lightweight, and low-power. The 0.07% mean RMS error in R_e is an improvement over the stationary bioimpedance system described previously, 0.4% [9], thus is expected adequate for portable residual limb fluid volume monitoring in free living environments. Clinical studies investigating R_i sensitivity to variables of interest are needed to determine if the 2.23% mean RMS error is sufficiently small for meaningful data interpretation.

Acknowledgements

Assistance from Sam Bennett and Horace Wang in manuscript revision is appreciated. This material is based upon work supported by the US Army Medical Research Acquisition Activity (USAMRAA) under Contract No. W81XWH-16-C-0020 and by the National Institutes of Health under Grant no. R01HD060585. Any opinions, findings and conclusions or recommendations expressed in this material are those of the authors and do not necessarily reflect the views of the USAMRAA or the National Institutes of Health.

Conflict of interest

None.

Ethical approval

Not required.

Supplementary materials

Supplementary material associated with this article can be found, in the online version, at doi:10.1016/j.medengphy.2019.04.002.

References

[1] Legro MW, Reiber G, del Aguila M, Ajax MJ, Boone DA, Larsen JA, Smith DG, Sangeorzan B. Issues of importance reported by persons with lower limb amputations and prostheses. J Rehabil Res Dev 1999;36:155–63.
[2] Zachariah SG, Saxena R, Fergason JR, Sanders JE. Shape and volume change in the transtibial residuum over the short term: preliminary investigation of six subjects. J Rehabil Res Dev 2004;41:683–94.
[3] Sanders JE, Severance MR, Allyn KJ. Computer-socket manufacturing error: how much before it is clinically apparent? J Rehabil Res Dev 2012;49:567–82.
[4] Youngblood RT, Hafner BJ, Allyn KJ, Cagle JC, Hinrichs P, Redd CB, Vamos AC, Ciol MA, Bean N, Sanders JE. Effects of activity intensity, time, and intermittent doffing on daily limb fluid volume change in people with transtibial amputation. Prosthet Orthot Int 2019;43:28–38.
[5] Sanders JE, Youngblood RT, Hafner BJ, Ciol MA, Allyn KJ, Gardner D, Cagle JC, Redd CB, Dietrich CR. Residual limb fluid volume change and volume accommodation: Relationships to activity and self-report outcomes in people with trans-tibial amputation. Prosthet Orthot Int 2018;42:415–27.
[6] Sanders JE, Youngblood RT, Hafner BJ, Cagle JC, McLean JB, Redd CB, Dietrich CR, Ciol MA, Allyn KJ. Effects of socket size on metrics of socket fit in trans-tibial prosthesis users. Med Eng Phys 2017;44:32–43.
[7] Sanders JE, Hartley TL, Phillips RH, Ciol MA, Hafner BJ, Allyn KJ, Harrison DS. Does temporary socket removal affect residual limb fluid volume of trans-tibial amputees? Prosthet Orthot Int 2016;40:320–8.
[8] Sanders JE, Redd CB, Cagle JC, Hafner BJ, Gardner DL, Allyn KJ, Harrison DS, Ciol MA. Preliminary evaluation of a novel bladder-liner for facilitating residual limb fluid volume recovery without doffing. J Rehabil Res Dev 2016;53:1107–20.
[9] Sanders JE, Moehring MA, Rothlisberger TM, Phillips RH, Hartley T, Dietrich CR, Redd CB, Gardner DW, Cagle JC. A bioimpedance analysis platform for amputee residual limb assessment. IEEE Trans Biomed Eng 2016;63:1760–70.
[10] Tucker AS, Fox RM, Sadleir RJ. Biocompatible, high precision, wideband, improved Howland current source with lead-lag compensation. IEEE Trans Biomed Circuits Syst 2013;7:63–70.
[11] Bao JZ, Davis CC, Schmukler RE. Impedance spectroscopy of human erythrocytes: system calibration and nonlinear modeling. IEEE Trans Biomed Eng 1993;40:364–78.
[12] De Lorenzo A, Andreoli A, Matthie J, Withers P. Predicting body cell mass with bioimpedance by using theoretical methods: a technological review. J Appl Physiol 1997;82:1542–58.
[13] Fenech M, Jaffrin MY. Extracellular and intracellular volume variations during postural change measured by segmental and wrist-ankle bioimpedance spectroscopy. IEEE Trans Biomed Eng 2004;51:166–75.
[14] Hanai T. Electrical properties of emulsions. In: Sherman P, editor. Emulsion science. London, England: Academic Press; 1968. p. 354–477.
[15] Aggarwal B, Gupta M, Gupta AK. A comparative study of various current mirror configurations: Topologies and characteristics. Microelectron J 2016;53:134–55.
[16] Langlois PJ, Neshatvar N, Demosthenous A. A sinusoidal current driver with an extended frequency range and multifrequency operation for bioimpedance applications. IEEE Trans Biomed Circuits Syst 2015;9:401–11.
[17] Chen DX, Deng X, Yang WQ. Comparison of three current sources for single-electrode capacitance measurement. Rev Sci Instrum 2010;81:034704-1–034704-3.
[18] Seoane F, Bragós R, Lindecrantz K. Current source for multifrequency broadband electrical bioipmedance spectroscopy systems. A novel approach. In: Proceedings of the IEEE EMBS Annual International Conference, New York City; 2006. Aug 30-Sep 3SaBP9.7.
[19] Toumazou C, Lidgey FJ, Makris CA. Extending voltage-mode amps to current–mode performance. IEE Proc G Circuits Device Syst 1990;137G:116–30.
[20] Yélamos D, Casas Ó, Bragós R, Rosell J. Improvement of a front end for bioimpedance spectroscopy. Ann NY Acad Sci 1999;873:306–12.
[21] Elwan HO, Soliman AM. Novel CMOS differential voltage current conveyor and its applications. IEEE Proc. Circuits Devices Syst 1997;144:195–200.
[22] Antonnsson EK, Mann RW. The frequency content of gait. J Biomech 1985;18:39–47.
[23] Sanders JE, Cagle JC, Allyn KJ, Harrison DS, Ciol MA. How do walking, standing, and resting influence transtibial amputee residual limb fluid volume? J Rehabil Res Dev 2014;51(2):201–12.